13

Image-Guided Transcatheter Aortic Valve Implantation Assistance System

Mohamed Esmail Karar[1], David Holzhey[2],
Matthias John[3], Ardawan Rastan[2],
Friedrich-Wilhelm Mohr[2] and Oliver Burgert[1]
[1]*Innovation Center Computer Assisted Surgery (ICCAS), University of Leipzig*
[2]*Department of Cardiac Surgery, Heart Center, University of Leipzig*
[3]*Siemens AG, Healthcare Sector, Forchheim*
Germany

1. Introduction

Transcatheter aortic valve implantation (TAVI) is a recently developed surgical technique to treat symptomatic aortic valve stenosis in elderly and high-risk patients (Eltchaninoff et al., 2008; Ferrari & von Segesser, 2010). Compared to the standard aortic valve replacement surgery, the TAVI limits the surgical access to either a small minithoracotomy (transapical TAVI) or femoral approach (transfemoral TAVI) causing minimal tissue trauma. Independently of the TAVI approach it can be performed on the beating heart without cardiopulmonary bypass support (Walther et al., 2009). Recovery time may be reduced and the patient can eventually return to normal activity more quickly. More than 70,000 transcatheter valve implantations have been performed worldwide (Valle-Fernández et al., 2010).

The TAVI is done via a retrograde (transfemoral, transaxillary) or antegrade (transapical) approach (Singh et al., 2008). The main advantage of the transapical TAVI technique is the direct access to the aortic valve which eliminates the need for a large peripheral vascular access in patients with peripheral vascular disease, small tortuous vasculature, a history of major vascular complications, or previous vascular interventions (Singh et al., 2008).

In transapical TAVI (Walther et al., 2009), a stented valve bioprosthesis that is temporarily crimped upon a balloon catheter, is inserted through the apex into the aortic root via a left anterolateral minithoracotomy. For that the apex of the left ventricle is punctured with a needle, and after balloon valvuloplasty the aortic valve prosthesis (AVP) is positioned within the stenotic aortic valve using guide wire techniques. After reaching the correct position, the stented AVP is deployed by an inflatable balloon to reach its final diameter, thus fixing the prosthesis to the aortic annulus (Fig. 1a).

The Edwards SAPIEN™ prosthesis (Edwards Lifesciences Inc, Irvine, CA, USA) is the most commonly used prosthesis for TAVI in several European countries and the only one approved for transapical approach so far (Thomas et al., 2010). Thus the Edwards SAPIEN™ prosthesis has been used in this study. It consists of three bovine pericardial cusps mounted into a stainless-steel balloon-expandable stent (Fig. 1b).

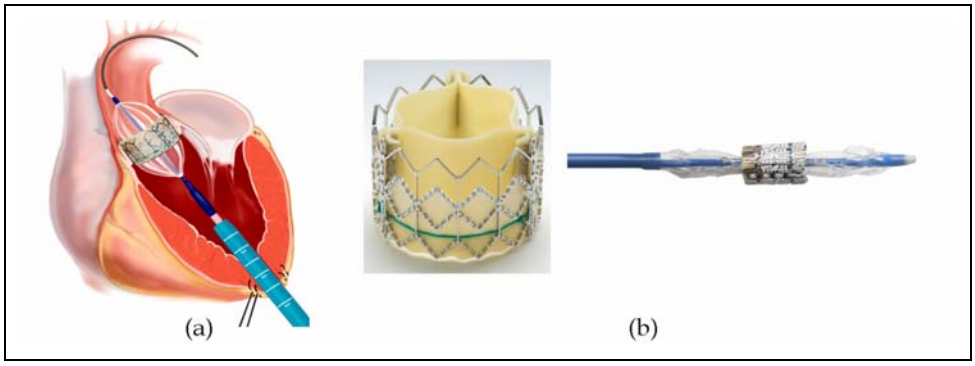

Fig. 1. Transcathete aortic valve implantation. (a) Schematic view of the transapical approach. (b) Edwards SPAIEN™ prosthesis and the balloon-based delivery system

Medical imaging technology, including computed tomography (CT), X-ray fluoroscopy, magnet resonance imaging (MRI), and echocardiography, is needed to provide accurate information on the stenotic valve and to choose the appropriate prosthetic valve size for TAVI procedures (Kaleschke et al., 2010; Van de Veire, 2010). Live two-dimensional (2D) X-ray fluoroscopy guidance is mostly used during the intervention, in order to determine proper valve positioning and the plane of alignment of the aortic valve cusps with supplemental echocardiography confirmation (Walther et al., 2009).
X-ray angiography and fluoroscopy C-arm imaging system (Siemens AG, Healthcare Sector, Forchheim, Germany) is recently used to capture both intraoperative three-dimensional (3D) C-arm CT images and live 2D fluoroscopic image sequences (Kempfert et al., 2009). At the begin of the surgical procedure, the physician uses the interventional C-arm imaging system to reconstruct a 3D CT image of the aortic root under a short episode of rapid ventricular pacing (RVP) from acquired rotational 2D image sequences by applying 75 ml diluted contrast agent of 200^{o} over 5 seconds (Fig. 2).

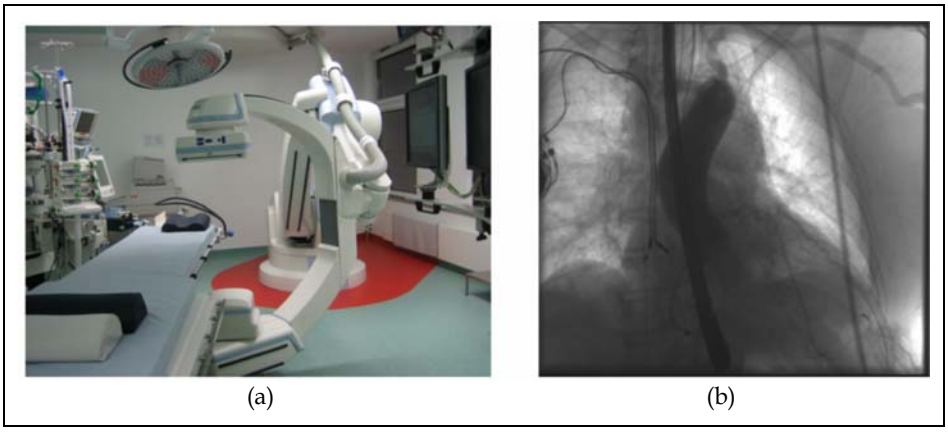

Fig. 2. (a) Angiography and fluoroscopy C-arm system (Artis Zeego, Siemens AG, Healthcare Sector, Forchheim, Germany). (b) Rotational angiographic scan such that 75 ml diluted contrast agent is injected into the aortic root, followed by 5 seconds run under rapid ventricular pacing

In the presence of contrast agent, different fluoroscopic projections are used to visualize the aortic root and the aortic annulus in a perpendicular view (Fig. 3a). The ventricular-aortic angle can only be estimated in the right anterior oblique (RAO) view, because the left anterior oblique (LAO) view looks at this angulation en face. The annular plane is sometimes visible depending on the amount of annular calcification, but often only indirect clues are provided by the position of a pigtail catheter. The pigtail catheter should be placed at the bottom of a coronary sinus. Information from planning CT or intraoperative C-arm CT images can be used to calculate the best possible fluoroscopic view for a coaxial implantation and automatically adjust the angulation of the C-arm without giving additional contrast agent. However, the following valve adjustment in the aortic annulus requires additional contrast injections and radiation exposure. When valve positioning is considered correct, the balloon-expandable prosthesis is released to replace the diseased valve under RVP as shown in Fig. 3b. After the implantation, the assessment of implanted AVP is also done using fluoroscopy guidance (Fig. 3c).

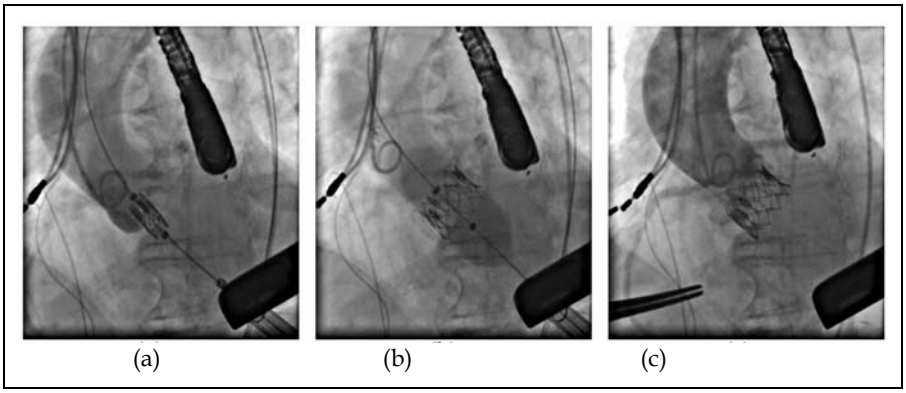

Fig. 3. 2D Fluoroscopy guidance during the transapical TAVI. (a) Valve positioning. (b) Valve implantation. (c) Final assessment after valve implantation

Exact valve placement is crucial during the intervention, because complications can arise from a misplaced valve, which are difficult to manage and requires different bailout strategies. These complications have been reported (Yan et al., 2010) such as high-degree atrioventricular (AV) block (10-30%), paravalvular leak (4-35%), coronary ostia occlusion (0.5-1%), aortic dissection (0-4%), cardiac tamponade (1-9%). A malposition of the prosthesis rarely occurs, however, 5.3% incidence (9/170) patients was reported (Al Ali et al., 2008). The 30-day mortality of the TAVI in Europe is 5-10 % (Thomas et al., 2010; Walther et al., 2010). Also, the contrast of fluoroscopic images is generally limited to minimize the radiation exposure for the patient and the physician. The contrast agent is injected to visualize the aortic root, valve annulus, and coronary ostia in few seconds. The amount of contrast injections must be minimized to avoid renal insufficiencies in high-risk elderly patients.

Only few previous studies deal with image-guided planning and intraoperative support of the TAVI procedure. Our research group has previously proposed a guidance system including a planning system (Gessat et al., 2009) and tracking the AVP in fluoroscopic image sequences (Karar et al., 2009, 2010). Siemens has prototypically equipped the interventional

C-arm with a system for automatic segmentation and overlay of aortic root volume and landmarks on 2D fluoroscopic images, but without motion correction (John et al., 2010). Robotic systems have been developed for the TAVI using intraoperative MRI guidance (Li et al., 2008, 2011). Real-time 3D transesophageal (TEE) is recently presented for guiding the TAVI (Siegel et al., 2011).

In order to potentially overcome the current difficulties associated with the TAVI under 2D fluoroscopy guidance, we present a new system that integrates a 3D aortic mesh model and landmarks form intraoperative C-arm CT images with tracking the prosthesis in live fluoroscopic images. The developed system is mainly based on image processing and visualization techniques, avoiding the use of additional implanted radiopaque markers or external tracking systems which may complicate the surgical workflow. Moreover, our system determines automatically a target area of implantation to allow the physician to identify the optimal position of the AVP without further contrast injections.

2. System overview

To assist the TAVI, our image-guided system is connected with the fluoroscopy C-arm system as depicted in Fig. 4. 2D fluoroscopic image sequences and a 3D geometrical mesh

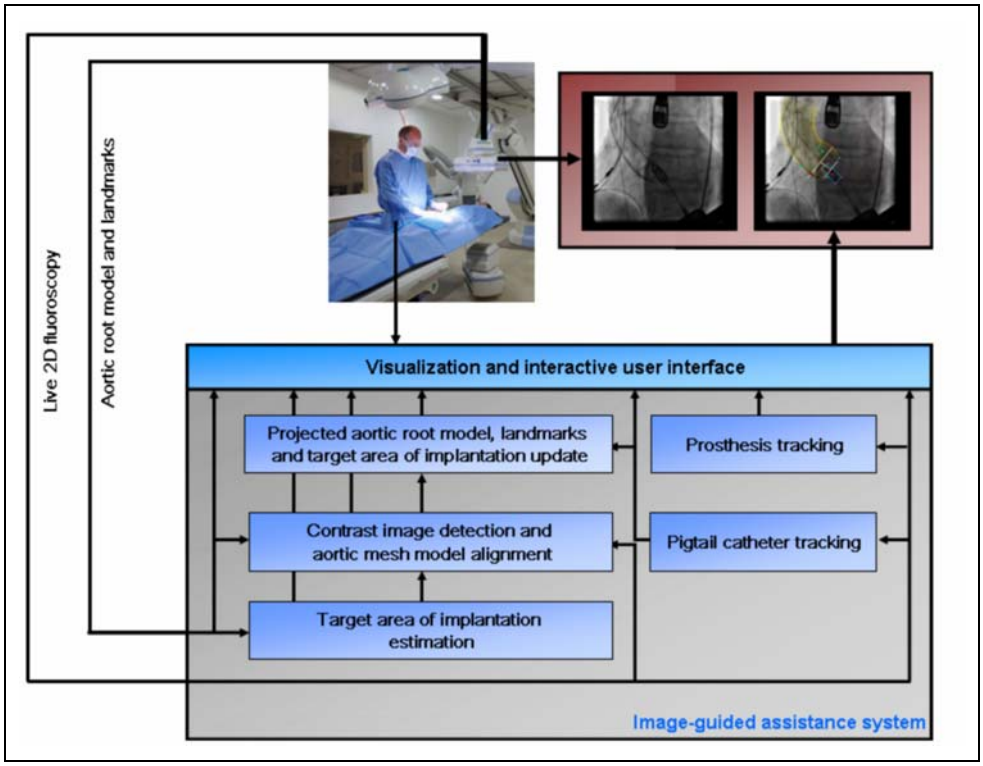

Fig. 4. Block diagram of the developed assistance system connected with the interventional C-arm imaging system for guiding the TAVI

model of the aortic root together with valve landmarks are acquired from the interventional C-arm system. A target area of valve implantation is automatically estimated inside the 3D mesh model based on the best experience and knowledge of the physician. The overlaid aortic mesh model, landmarks, and estimated target area of implantation are updated onto 2D fluoroscopic images by approximating the translational motion of the aortic root without contrast injections from the pigtail catheter motion. In parallel, the prosthesis is also tracked to assist the positioning of AVP within the clinical accepted margins.

2.1 Target area of implantation estimation

The 3D geometrical mesh model of the aortic root and eight anatomical landmarks of the stenotic valve are generated based on an automatic segmentation of the aortic root in intraoperative C-arm CT images (Zheng et al., 2010). The eight landmark points are the two points of coronary ostia [left and right], the three points of commissures [left, right, and non-coronary], and the three lowest points (hinge points) of each leaflet cusp [left, right, and non-coronary]

The correct position of the AVP should be 1/3 to 1/2 of its length above and perpendicular to the aortic annulus (Walther et al., 2009). In this study, the target area of valve implantation is automatically defined by two embedded circles of the annulus and ostia planes with the normal center line to the annulus (Gessat et al., 2009). Fig. 5a shows the aortic mesh model, landmarks and estimated target area of implantation.

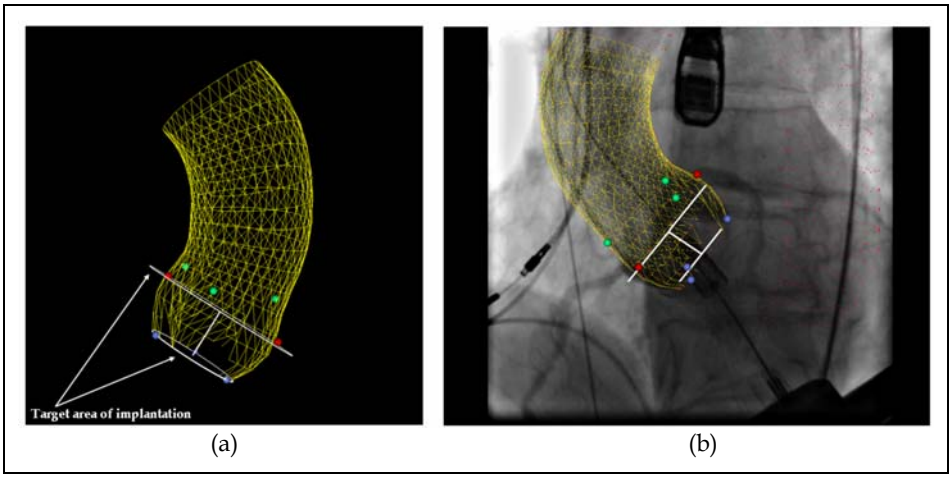

Fig. 5. (a) 3D model of the aortic root (yellow meshes) and valve landmarks as colored points; namely coronary ostia (red), commissures (green) and lowest points of the leaflets cusps (blue) and estimated target area of the valve implantation (white). (b) Alignment of the projected model and landmarks with a contrast image

2.2 Contrast image detection and aortic mesh model alignment

Automatic detection of contrast agent in a fluoroscopic image is used to initialize the synchronized mesh model tracking with aortic root motion in interventional image sequences. Enhanced contrasted aortic root shows up dark pixels in the entire aorta roadmap if the contrast agent is injected. By analyzing the histogram and using the 98-percentile as a

threshold measure of contrast agent, the enhanced contrast image is automatically detected after learning histogram feature curve of the first 20 images of sequence without contrast agent (Condurache et al., 2004).
The aortic mesh model, valve landmarks and target area of implantation are projected to the fluoroscopic image plane using the transformation matrix of interventional C-arm imaging system. They are manually aligned to the contrast image as shown in Fig. 5b.

2.3 Pigtail catheter tracking for approximating aortic root motion

Fluoroscopic images are pre-processed using a 2-D Gabor filter (Kong et al., 2003), in order to reduce the image noise and adjust intensities within the sequence while preserving the important pigtail features.
The position of the pigtail catheter is detected in all image sequences using the template matching approach (Briechle & Hanebeck, 2001). The template image of the pigtail catheter *t* is manually defined on the first image of sequence. A region of interest (ROI) of the image is defined to reduce the processing time and increase the algorithm robustness. In practice, the size of the ROI is 2.5 times the size of the template image and is constant for all images of each sequence.
In this approach, I(x,y) denotes the intensity of a preprocessed ROI image of the size $S_x \times S_y$ at point (x, y), $x \in \{0, ..., S_x\text{-}1\}$, $y \in \{0, ..., S_y\text{-}1\}$ and the template image t of the size $s_x \times s_y$. The position of catheter is determined by a pixelwise comparison of the ROI image with the target window based on the computing of fast normalized cross correlation coefficient γ at each point (u, v) for ROI and template images. Eq. 1 gives the definition of γ. $\bar{i}_{u,v}$ and $\bar{t}$ are the mean brightness values within the ROI and the template image respectively. The normalized maximal value γ_{max} at the point (u, v) in the current ROI image defines the best matching location of the template.

$$\gamma(u,v) = \frac{\sum_{x,y}[I(x,y) - \bar{i}_{u,v}][t(x-u,y-v) - \bar{t}]}{\sqrt{\sum_{x,y}[I(x,y) - \bar{i}_{u,v}]^2 \sum_{x,y}[t(x-u,y-v) - \bar{t}]^2}} \tag{1}$$

The global translational motion of aortic mesh model is then updated during the intervention by calculating the updated displacement of pigtail catheter between two frames such that the difference between the matching locations of template in one frame and the corresponding template position in the other frame defines the 2D displacement of the pigtail catheter.
We assumed that the tracking of the aortic mesh model could be automatically stopped in the images with or without contrast injections if the best matching value of γ_{max} is less than 50%, avoiding the failure of template-based tracking algorithm.

2.4 Prosthesis tracking

Real-time tracking of the AVP is performed by using template matching approach to estimate the position of the AVP and a shape model of the prosthesis to extract the corner points of the AVP in fluoroscopic image sequences (Karar et al., 2010). To start the AVP tracking procedure, an initialization step is performed by manually defining the corner points of the prosthesis in the first image of sequence to provide the required algorithm parameters which are prosthesis model parameters and a target window including the template image of the AVP.

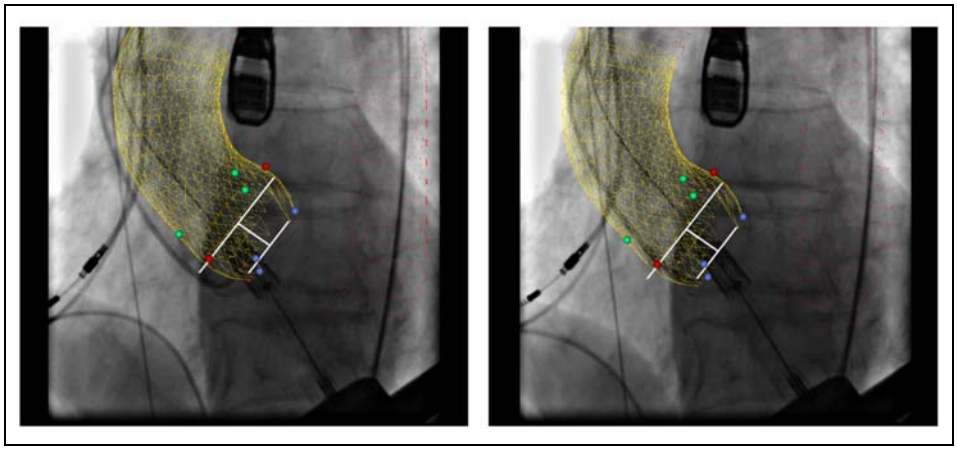

Fig. 6. Overlay of aortic mesh model, landmarks and target area of implantation onto a fluoroscopic image of sequence without updating (a) and with updating via pigtail catheter tracking (b)

The geometrical parameters of the model of the prosthesis are estimated. Fig. 7a shows the AVP model which is defined as a semi-rectangle with the height h. The upper and lower widths are w_1 and w_2 respectively. Corner points are noted p_1, p_2, p_3, and p_4. The prosthesis's angle φ is defined between the two segments (p_1-p_2) and (p_1-p_4). The angle θ between (p_c-p_1) and the horizontal line represents the orientation of the prosthesis in the current image. The measures h, w_1, w_2 and φ are assumed to be constant for all images in the sequence and just before inflating the balloon to reach the prosthesis's final diameter.
The target window of the prosthesis image is automatically defined around AVP corner points such that the height and the width of the target window are $|p_{4y} - p_{2y}|$ and $|p_{3x} - p_{1x}|$ with one pixel offset to get the complete image of AVP respectively.
Similar to template-based tracking algorithm of pigtail catheter, the prosthesis template image is detected within all images of the sequence. We proposed using the prosthesis model (Fig. 7a) to perform AVP corner points localization as follows: The target window always shows the corner point p_1 of the prosthesis at the maximum x-coordinate value in the image plane which is detected by Canny filter edge detection (Canny, 1986).
In Fig. 7a, the angle θ in the current image i is determined between (p_c-p_1) line and the horizontal line. The prosthesis center p_c is obtained using template matching. The orientation difference $\Delta\theta_i$ represents the rotation angle of the prosthesis, calculated between the current orientation in a processed image θ_i and the initial orientation in the first image of sequence θ_1. The initial AVP orientation θ_1 is used as a reference orientation angle to minimize the distance errors of prosthesis tracking in the image sequences as follows:

$$\Delta\theta_i = \theta_i - \theta_1, \quad i = 2 \ldots n \tag{2}$$

Then the new positions of three corner points namely p_2, p_3 and p_4 are obtained by rotating the position of AVP model in the first image with $\Delta\theta_i$. Finally, the tracked prosthesis is displayed linking the four corner points on the current image of sequence (Fig. 7b).

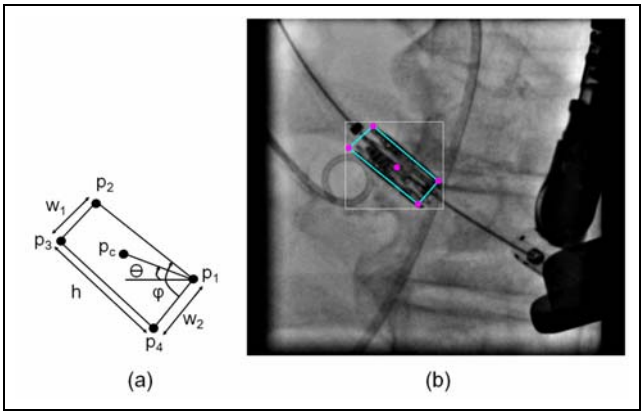

Fig. 7. (a) Prosthesis shape model. (b) Tracked prosthesis inside the target window onto a fluoroscopic image

2.5 Visualization and interactive user interface

An interactive graphical user interface (GUI) has been implemented to be integrated with the proposed method based on visual C++ programming language. Different views of projected mesh model, landmarks and target area of implantation are separately visualized to allow the physician to display only the required information for the prosthesis deployment (Fig. 8). Using the developed GUI, the localization errors of model projection as well as tracking of aortic mesh model and AVP can be also manually minimized if occur.

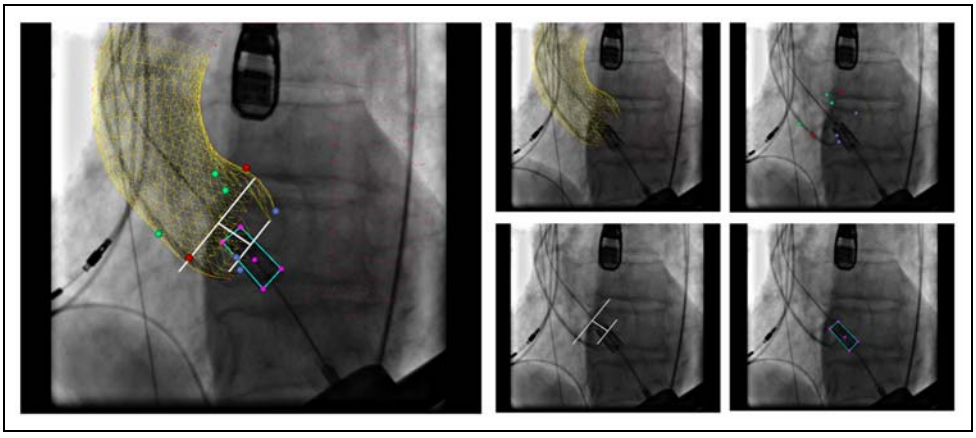

Fig. 8. Different visualization views of the projected aortic mesh model, landmarks, target area of implantation and tracked prosthesis onto a fluoroscopic image

The parameter values needed to compute the 3D-2D transformation matrix of the C-arm imaging system are imported from a fluoroscopic DICOM (Digital Imaging and Communications in medicine) file or given by the user. A template image of pigtail catheter and alignment of projected mesh model to the contrast image are manually defined before tracking of the catheter.

3. Experiments and evaluation

3.1 Experimental setup

We have tested the image-guided assistance system in a hybrid operating room at the Heart Center, University of Leipzig, Germany (Fig. 9). The hybrid operating room is a special operating room equipped with angiography and fluoroscopy C-arm system (Artis Zeego, Siemens AG, Healthcare Sector, Forchheim, Germany) and offering all surgical prerequisites such as sterile valve preparation before implantation, anaesthetic equipment, appropriate lighting, and the heart-lung machine as a backup to perform a safe TAVI procedure (Nollert & Wich, 2009; Pasic et al., 2010).

The assistance system is a PC (Intel® Core™ Quad CPU 2.4 GHz, 3.25 GB RAM) equipped with our guidance software that is able to capture live fluoroscopy video images via the Matrox Helios eA/XA frame grabber card. The Siemens C-arm system sends fluoroscopy images to our assistance system workstation over multi-mode optical fiber cables, DVI-D/VGA adapter, and a video-switcher. The captured fluoroscopic images are 1280x1024 pixels.

To start the experiment, 3D aortic mesh model and valve landmarks are reconstructed on a Siemens Workstation from the corresponding 3D DynaCT images and saved on an USB-stick as SEG (Society of Exploration Geophysicists) files to be read by the image-guided assistance system.

Fig. 9. Integration of image-guided TAVI assistance system in the hybrid operating room

3.2 Patient datasets and results

Experiments were retrospectively performed on ten patient datasets from clinical routine of the TAVI. Each patient dataset include a fluoroscopic image sequence and the related aortic mesh model with valve landmarks. The fluoroscopic sequences include 70-100 images per sequence with 512 × 512 to 1024 × 1024 pixels. The pixel size was approximately 0.2 mm. Fig. 10 shows assistance system results for a sample of three different datasets.

The initialization step for defining a template image of pigtail catheter, template image of the AVP, importing 3D aortic mesh model with landmarks including estimated target area of implantation and its alignment with detected contrast image varied between three to five minutes. The total computation time for fluoroscopic image processing algorithms was approximately 100 milliseconds per frame.

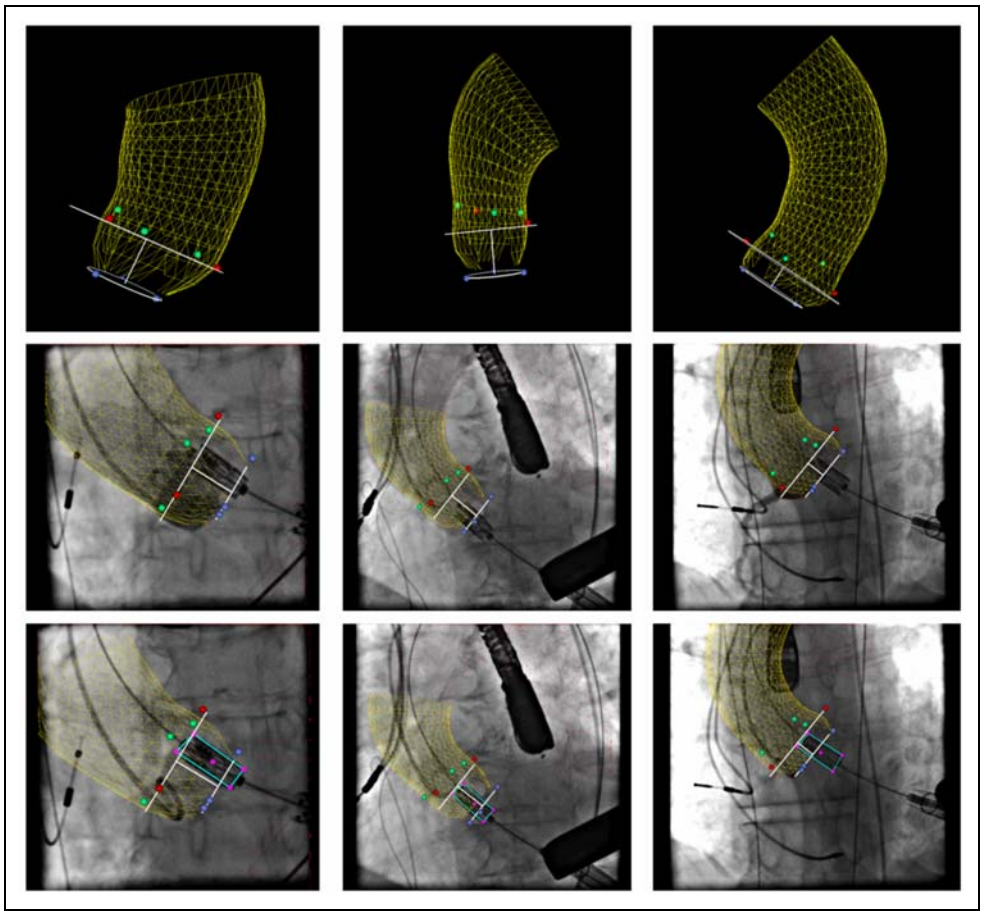

Fig. 10. Examples of the developed system results. First row: aortic mesh models with landmarks and estimated target area of implantation. Second row: Alignment of projected aortic mesh models with detected contrast images. Third row: Updating of visualized models based on tracked aortic pigtail catheter without contrast injections

3.3 Evaluation

3.3.1 Methods

The developed assistance system's guidance accuracy was determined by the tracking accuracy of both the pigtail catheter and the AVP. In each image of all tested datasets, the tracking accuracy was assessed by computing the absolute displacement errors between the

automatically and manually located pigtail's template and two upper corner points of the prosthesis p_2 and p_3, because the upper side of prosthesis (p_2-p_3) must be positioned below the coronary ostia. For each image *i* of the sequence, the automatic localization target point (x_i^A, y_i^A) and manual localization target point (x_i^M, y_i^M) are used to compute the displacement error d_i. The absolute mean error d_{mean} ± standard deviation (SD) and maximum error d_{max} are also computed over n images of the sequence as:

$$d_i = \sqrt{(x_i^A - x_i^M)^2 + (y_i^A - y_i^M)^2} \tag{3}$$

$$d_{mean} = \frac{\left(\sum_{i=1}^{n} d_i\right)}{n} \tag{4}$$

$$d_{max} = \max_i |d_i| \tag{5}$$

3.3.2 Results

Figure 11 shows the evaluation results of the tracked pigtail catheter for ten fluoroscopic image sequences, excluding the images with high dose contrast injections (3-10 images per each sequence) which temporarily switch off the tracking procedure of the pigtail catheter. Seq . 1 shows relatively high displacement errors d_{mean} = 1.73 ± 0.86 mm and d_{max} = 4.37 mm because the pigtail catheter had been slightly repositioned by the physician, Seq. 7 and Seq. 8 present the highest maximum displacement errors 4.65 mm and 4.84 mm respectively. However, all tested fluoroscopic images showed that the maximum and mean displacement errors of the pigtail tracking were less than 5.0 mm for one to three images per each sequence only and less than 2.0 mm respectively. These error values remain within the clinical accepted range.

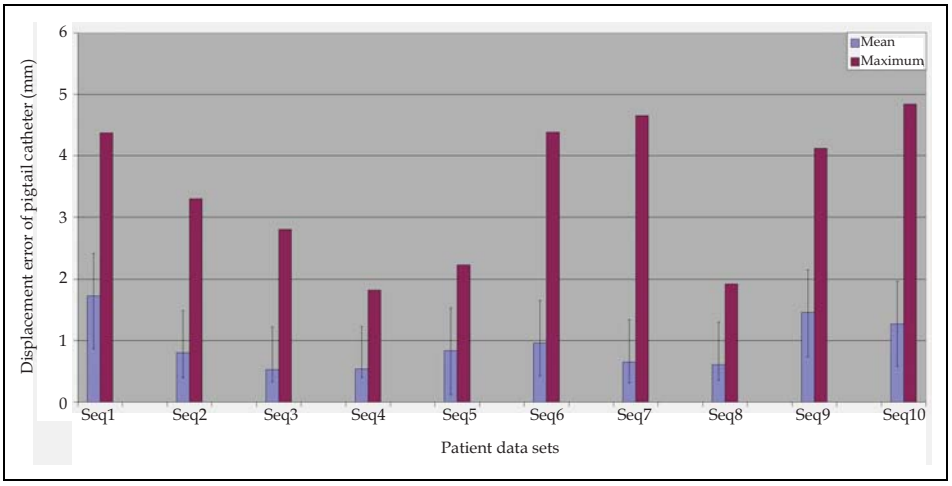

Fig. 11. Evaluation tracking results of the pigtail catheter for ten fluoroscopic image sequences. The maximum errors are less than 5.0 mm only for one to three images per sequence, while the absolute mean errors are less than 2.0 mm for all tested fluoroscopic images

The displacement errors of the prosthesis corner points p_2 and p_3 are depicted in Fig. 12. The mean errors of p_2 and p_3 were approximately similar and varied from 0.26 ± 0.05 to 0.42 ± 0.06 mm. Because the images of Seq. 1 and Seq. 7 have been captured at low contrast agent doses in the images, the lowest localization errors were obtained ($d_{max} \leq 0.3$ mm). The maximum localization error of p_2 and p_3 was less than 0.5 mm in all tested image sequences.

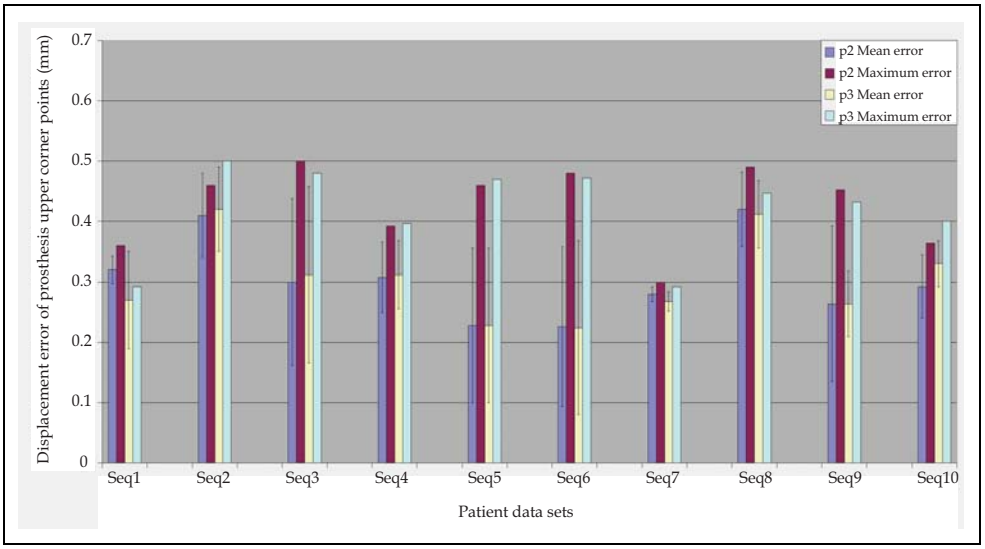

Fig. 12. Evaluation tracking results of two upper corner points of the prosthesis p_2 and p_3. The maximum displacement errors of two corner points p_2 and p_3 are less than 0.5 mm in all tested fluoroscopic images

4. Discussion

For validation purposes, the experiments of our assistance system were performed using a Siemens angiography and fluoroscopy C-arm system in the hybrid operating room. The tracking accuracies of the pigtail catheter and upper corner points of the AVP were determined to evaluate the system performance. The failure in one image of sequence could occur during template-based tracking procedures and corrected in the next image of the same sequence. As depicted in Fig. 11 and Fig. 12, the evaluation results showed that the mean overlay errors are less than 2.0 mm based on displacement errors of the pigtail catheter, while the maximum localization errors of the upper corner points p_2 and p_3 of AVP are less than 0.5 mm. The resulting errors are within the clinical accepted margins for all tested fluoroscopic images.

We demonstrated that a fast approach to track successfully the pigtail catheter without contrast agent injection and the prosthesis with using a shape model, see Fig. 7. The pigtail catheter tracking is only stopped during the contrast injection, because the overlay is not required and should be switch off if the contrast agent appears in fluoroscopic images (Condurache et al., 2004). For the AVP tracking, the prosthesis detection can be affected by

possible rotation of the prosthesis ($\Delta\theta_i$) and the presence of contrast agent. But the template matching algorithm is still robust enough in finding the correct position of AVP in all tested fluoroscopic images.

In summary, our image-guided TAVI assistance system has been developed to assist the positioning of the AVP under live 2D fluoroscopy guidance. To allow continuous visualization of diseased valve without further contrast injections, the projected 3D aortic root mesh model and landmarks from intraoperative C-arm CT images are overlaid and updated onto fluoroscopic images according to the aortic root motion via tracking the pigtail catheter. Moreover, the AVP is tracked to align with the estimated target area of implantation. Interactive user interface is integrated with the image-guided TAVI assistance system to ensure the safe guidance procedures of the TAVI.

5. Conclusion

The developed fluoroscopy-guided TAVI assistance system aims to guide the physician to accurately define the exact position of the AVP. Only a minimal user-interaction is required for initializing the image processing algorithms and visually correcting possible displacement errors of projected aortic shape model and AVP during the intervention if needed. In addition to the transapical TAVI discussed here, the assistance system can be also applied for the transfemoral approach. Now, the developed assistance system is undergoing evaluation during real-time TAVI intervention.

6. Acknowledgement

The authors would like to thank Alois Nöttling and Stefan Ammon for the technical support to obtain the experimental imaging data. The authors also thank Petra Bergmann, Frank Wüst, and Michael Heinze from Edwards Lifesciences Inc. for providing the images of Edwards-SPAIEN prosthesis for this study. We gratefully thank Prof. Volkmar Falk from University Hospital Zurich and Dr. Claire Chalopin from Innovation Ceneter Computer Assisted Surgery (ICCAS) for their comments and fruitful discussions. This work is supported by German Academic Exchange Service (DAAD) in cooperation with the Egyptian Supreme Council of Universities (ESCU) under scholarship number A0690520. This work is partially funded by Siemens Healthcare AG, Forchheim, Germany.

7. References

Al Ali, A. M., Altwegg, L., Horlick, E. M., Feindel, C., Thompson, C. R., Cheung, A., Carere, R. G., Humphries, K., Ye, J., Masson, J. B. & Webb, J. G. (2008). Prevention and Management of Transcatheter Balloon-Expandable Aortic Valve Malposition. *Catheter Cardiovasc Interv*, Vol.72, No.4, (October 2008), pp. 573-578, DOI 10.1002/ccd.21667

Briechle, K. & Hanebeck, U. D (2001). Template Matching Using Fast Normalized Cross Correlation. *Proceedings of SPIE 2001 International Conference on Optical Pattern Recognition XII,* Vol.4387, pp. 95-102, DOI 10.1117/12.421129, Orlando, Florida, USA, 19 April, 2001

Canny, J. (1986). A Computational Approach to Edge Detection. *IEEE Trans. Pattern Anal. Mach. Intell.*, Vol.8, No.6, (November 1986), pp. 679-698, ISSN 0162-8828

Condurache, A. P., Aach, T., Eck, K. & Bredno, J. (2004). Fast Detection and Processing of Arbitrary Contrast Agent Injections in Coronary Angiography and Fluoroscopy. *Presented at Bildverarbeitung für die Medizin 2004 (Algorithmen, Systeme, Anwendungen)*, pp. 5-9, ISBN 978-3-540-21059-7, Berlin, Germany, March 29-30, 2004

Eltchaninoff, H., Zajarias, A., Tron, C., Litzler, P. Y., Baala, B., Godin, M., Bessou, J. P. & Cribier, A. (2008). Transcatheter Aortic Valve Implantation: Technical Aspects, Results and Indications. *Arch Cardiovasc Dis*, Vol.101, No.2, (February 2008), pp. 126-132, ISSN 1875-2136

Ferrari, E. & von Segesser, L. K. (2010). Transcatheter Aortic Valve Implantation (TAVI): State of the Art Techniques and Future Perspectives. *Swiss Med Wkly*, Vol. 140, (December 2010), pp. w13127, ISSN 0036-7672

Gessat, M., Merk, D. R., Falk, V., Walther, T., Jacobs, S., Nottling, A. & Burgert, O. (2009). A Planning System for Transapical Aortic Valve Implantation. *Proceedings of SPIE Medical Imaging 2009: Visualization, Image-Guided Procedures, and Modeling*, Vol.7261, pp. 72611E, DOI 10.1117/12.810270, Orlando, Florida, USA, February 8, 2009

John, M., Liao, R., Zheng, Y., Nottling, A., Boese, J., Kirschstein, U., Kempfert, J. & Walther, T. (2010). System to Guide Transcatheter Aortic Valve Implantations Based on Interventional C-arm CT Imaging. *Med Image Comput Comput Assist Interv*, Vol. 13, No. Pt 1, (2010), pp. 375-382, DOI 10.1007/978-3-642-15705-9_46

Kaleschke, G., Seifarth, H., Kerckhoff, G., Reinecke, H. & Baumgartner, H. (2010). Imaging Decision-Making for Transfemoral or Transapical Approach of Transcatheter Aortic Valve Implantation. *EuroIntervention : journal of EuroPCR in collaboration with the Working Group on Interventional Cardiology of the European Society of Cardiology*, Vo. 6, Suppl. G, (June 2010), pp. G20-27, ISSN 1774-024X

Karar, M. E., Gessat, M., Walther, T., Falk, V. & Burgert, O. (2009). Towards A New Image Guidance System for Assisting Transapical Minimally Invasive Aortic Valve Implantation. *Conf Proc IEEE Eng Med Biol Soc* 2009, pp. 3645-3648, Minneapolis, Minnesota, USA, Septemper 3-6, 2009, ISSN 1557-170X

Karar, M. E., Merk, D. R., Chalopin, C., Walther, T., Falk, V. & Burgert, O. (2010). Aortic Valve Prosthesis Tracking for Transapical Aortic Valve Implantation. *Int J Comput Assist Radiol Surg*. (September 2010), pp. 1-8, ISSN 1861-6410

Kempfert, J., Falk, V., Schuler, G., Linke, A., Merk, D., Mohr, F. W. & Walther, T. (2009). Dyna-CT During Minimally Invasive Off-Pump Transapical Aortic Valve Implantation. *Ann Thorac Surg*, Vol. 88, No. 6, (December 2009), pp. 2041, ISSN 0003-4975

Kong, W. K., Zhang, D. & Li, W. (2003). Palmprint Feature Extraction Using 2-D Gabor Filters. *Pattern Recognition*, Vol. 36, No. 10, (October 2003), pp. 2339-2347, ISSN 0031-3203

Li, M., Kapoor, A., Mazilu, D. & Horvath, K. A. (2011). Pneumatic Actuated Robotic Assistant System for Aortic Valve Replacement Under MRI Guidance. *Biomedical*

Engineering, IEEE Transactions on, Vol. 58, No. 2, (January 2011), pp. 443-451, ISSN 0018-9294

Li, M., Mazilu, D. & Horvath, K. (2008). Robotic System for Transapical Aortic Valve Replacement with MRI Guidance. *Medical Image Computing and Computer-Assisted Intervention*. Vol. 5242, (2008), pp. 476-484, DOI: 10.1007/978-3-540-85990-1_57

Nollert, G. & Wich, S. (2009). Planning A Cardiovascular Hybrid Operating Room: The Technical Point of View. *The heart surgery forum*, Vol.12, No. 3, (June 2009), pp. E125-130, ISSN 1098-3511

Pasic, M., Unbehaun, A., Dreysse, S., Drews, T., Buz, S., Kukucka, M., Mladenow, A., Gromann, T. & Hetzer, R. (2010). Transapical Aortic Valve Implantation in 175 Consecutive Patients: Excellent Outcome in Very High-Risk Patients. *Journal of the American College of Cardiology*, Vol. 56, No.10, (August 2010), pp. 813-20, ISSN 0735-1097

Siegel, R., Luo, H. & Biner, S. (2011). Transcatheter Valve Repair/Implantation. *The International Journal of Cardiovascular Imaging (formerly Cardiac Imaging)*, pp. 1-13, ISSN 1569-5794

Singh, I. M., Shishehbor, M. H., Christofferson, R. D., Tuzcu, E. M. & Kapadia, S. R. (2008). Percutaneous Treatment of Aortic Valve Stenosis. *Cleveland Clinic journal of medicine*, Vol.75, No.11, (November 2008), pp. 805-812, DOI 10.3949/ccjm.75.11.805

Thomas, M., Schymik, G., Walther, T., Himbert, D., Lefevre, T., Treede, H., Eggebrecht, H., Rubino, P., Michev, I., Lange, R., Anderson, W. N. & Wendler, O. (2010). Thirty-Day Results of the SAPIEN Aortic Bioprosthesis European Outcome (SOURCE) Registry: A European Registry of Transcatheter Aortic Valve Implantation Using the Edwards SAPIEN Valve. *Circulation*, Vol. 122, No.1, (July 2010), pp. 62-69, DOI 10.1161/circulationaha.109.907402

Valle-Fernández, R. d., Martinez, C. A. & Ruiz, C. E. (2010). Transcatheter Aortic Valve Implantation. *Cardiology Clinics*, Vol.28, No.1, (February 2010), pp. 155-168, ISSN 0733-8651

Van de Veire, N. (2010). Imaging to Guide Transcatheter Aortic Valve Implantation. *Journal of Echocardiography*, Vol. 8, No.1, (March 2010), pp. 1-6, ISSN 1349-0222

Walther, T., Dewey, T., Borger, M. A., Kempfert, J., Linke, A., Becht, R., Falk, V., Schuler, G., Mohr, F. W. & Mack, M. (2009). Transapical Aortic Valve Implantation: Step by Step. *Ann Thorac Surg*, Vol. 87, No. 1, pp. 276-83, ISSN 0003-4975

Walther, T., Schuler, G., Borger, M. A., Kempfert, J., Seeburger, J., Rückert, Y., Ender, J., Linke, A., Scholz, M., Falk, V. & Mohr, F. W. (2010). Transapical Aortic Valve Implantation in 100 Consecutive Patients: Comparison to Propensity-Matched Conventional Aortic Valve Replacement. *European Heart Journal*, Vol.31, No.11, (January 2009), pp. 1398-1403, DOI 10.1093/eurheartj/ehq060

Yan, T. D., Cao, C., Martens-Nielsen, J., Padang, R., Ng, M., Vallely, M. P. & Bannon, P. G. (2010). Transcatheter Aortic Valve Implantation for High-Risk Patients with Severe Aortic Stenosis: A Systematic Review. *The Journal of thoracic and cardiovascular surgery*, Vol.139, No.6, (Junary 2010)pp. 1519-28, ISSN 0022-5223

Zheng, Y., John, M., Liao, R., Boese, J., Kirschstein, U., Georgescu, B., Zhou, S. K., Kempfert, J., Walther, T., Brockmann, G. & Comaniciu, D. (2010). Automatic Aorta Segmentation and Valve Landmark Detection in C-arm CT: Application to Aortic Valve Implantation. *Med Image Comput Comput Assist Interv*, Vol. 13, No. Pt 1, pp. 476-83, DOI 10.1007/978-3-642-15705-9_46